III European Conference on Computational Mechanics
Solids, Structures and Coupled Problems in Engineering
C.A. Mota Soares et.al. (eds.)
Lisbon, Portugal, 5–8 June 2006

A PHENOMENOLOGICAL MODEL TO SIMULATE MECHANICAL TESTS ON ULTRAFINE-GRAINED ALUMINUM PRODUCED BY ECAE

B. Diouf [1], F. El Houdaigui[1], S. Poortmans [2], B. Verlinden[2] and A. M. Habraken [1]

[1] Department of Mechanics of Materials and Structures
University of Liège, chemin des Chevreuils 1, 4000 Liège, Belgium
{bdiouf, felhoudaigui, Anne.Habraken}@ulg.ac.be

[2] Departement of Materials Engineering
Katholieke Universiteit Leuven, Kasteelpark Arenberg 44, 3001 Leuven, Belgium
{Stijn.Poortmans, Bert.Verlinden}@mtm.kuleuven.be

Keywords: Aluminum, Equal Channel Angular Extrusion (ECAE), model identification.

Abstract. *Results of FEM simulations predicting the mechanical behavior at room temperature of test specimens of ultrafine-grained aluminum produced by ECAE are presented. The constitutive law is either based on a Hill model or on the Minty micro-macro model and coupled with an isotropic hardening law and/or kinematic hardening law.*

The yield locus shape, its size and its position during tension, compression and torsion tests have been studied. Initial texture measurements allow the identification of a constitutive law based on a set of representative crystals and crystal plasticity approach using a Full-Constraint Taylor model.
Finite element simulations using the previous constitutive laws are compared with experimental investigations. The results show that applying an initial back stress identified by tensile and compression tests to the yield locus predicts the initial flow stress in torsion test. The Minty micro-macro model coupled with a Voce type hardening model gives a good agreement with experimental results for the prediction of the shape at different stages of deformation of a compressed test specimen.
The simulation of tensile tests underline the need of inverse modeling as, due to the test specimen shape, the test is far from being homogeneous. The link between test specimen length and the necking appearance is studied.

1 INTRODUCTION

Equal Channel Angular Extrusion is a way to decrease the grain size in metallic materials. Due to the large plastic deformations, work hardening and grain refinement happen and the produced material has an increased strength. An additional annealing treatment can restore both ductility and work hardening behavior, while stabilizing the microstructure.

The material behavior requires a specific modeling as the monotonic tests show that the material anisotropy has evolved during the ECAE process and that the hardening phenomena seem different during tensile and compression tests (Figure 1a). In a first approach, an elasto plastic constitutive law models the experimental results as for strain rates higher than 10^{-2} s^{-1} the strain rate effect seems to have no effect for the chosen material. However looking at lower strain rates, a viscous effect appeared; it modifies the stress level and affects the necking appearance in the tensile state.

The current paper summarizes three investigated models. The first one is the Hill 1948 well known law, which allows modeling the initial plastic yield value in compression, tension and torsion. Coupled with a hardening model, it provides an approximative prediction of the behavior in compression. The second model relies on a more complex description of the yield locus shape; it improves the prediction of the deformed shape during a large strain compression test.

In order to extend these constitutive laws to model the hardening tensile behavior, the tensile experiments have been analyzed. The first simulations with simple isotropic elasto-plastic law have directly demonstrated the non homogeneity of the test and that for slow tests the strain rate effect cannot be neglected. Preliminary results are presented even if a satisfactory macroscopic model able to model all the monotonic tests is not yet achieved.

2 EXPERIMENTAL

Hot rolled commercial aluminum AA1050 was investigated in this study. The initial grain size is about 100µm. In order to obtain an ultrafine-grained (UFG) material, test specimen of 12mm in diameter and 60mm in length were subjected to equal channel angular extrusion at room temperature (RT), following route B_C for 8 passes [1]. The final grain size was about 1µm.

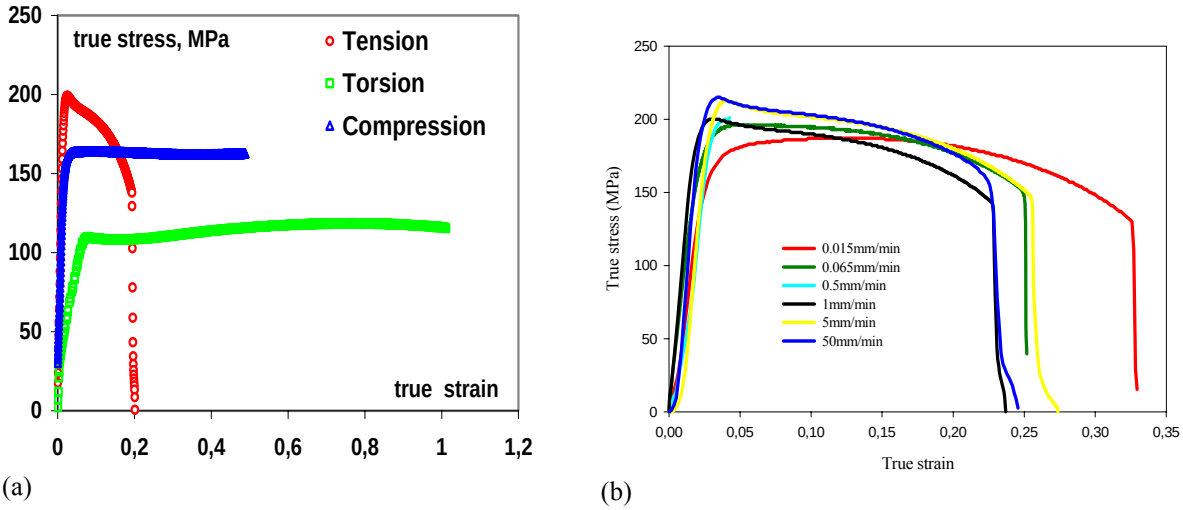

Figure 1: (a) Tensile and compression true stress-true strain curves and torsion (τ-γ) curve of Al-ECAE for strain rate higher than 10^{-2} s^{-1}; (b) effect of test speed in the true stress-true strain tensile curve.

To characterize the ECAE material, uniaxial tensile, compression and torsion tests were carried out at room temperature. This first set of tests was performed in a strain rate range higher than 10^{-2} s^{-1}.The tensile and compression stress-strain were directly computed from force-displacement measurement assuming homogeneous stress and strain fields and taking into account a section defined by volume preservation. The well known Nadaï formula [2] provides the stress-strain curve in torsion.
These true stress-true strain curves are shown in Figure 1a. A second set of tensile experiments conducted at slower strain rate were performed. The test velocity is constant, meaning that the strain rate evolves during the test. Figure 1b shows the computed stress-strain curves still assuming stress homogeneity in the test specimens. In this case, strain rate sensitivity is clearly observed for the slower strain rates. Note that according test specimen geometry a tensile test velocity of 0.015mm/sec, 0.065mm/sec, 0.5 mm/sec, 1 mm/sec, 5 mm/sec, 50 mm/sec respectively means an initial strain rate of $1.5{\cdot}10^{-5}s^{-1}$, $10^{-4}s^{-1}$, $8{\cdot}10^{-4}s^{-1}$, $10^{-3}s^{-1}$, $10^{-2}s^{-1}$, $\cdot 10^{-1}s^{-1}$.

3 MODELLING

To model mechanical tests, the finite element code Lagamine [3] has been used. As torsion and compression tests were performed in the strain rate higher than 10^{-2} s^{-1}, and that the tensile test experiments (Figure 1b) confirm that for this strain rate range no strain rate effect is observed, the first identified models were elasto-plastic ones. The yield locus is either based on the Hill 1948 model or on the Minty micro-macro model [4] and it is coupled with an isotropic Voce hardening law and/or a kinematic hardening law.

3.1 Shape and position of yield locus

For the initial aluminum sheet and the ECAE material, the crystallographic texture was measured and the corresponding Taylor-Bishop-Hill (TBH) yield locus was computed with a Taylor approach applied on a set of 2000 representative crystal orientations [5]. Figure 2b shows the anisotropy evolution introduced by the ECAE process. The Lankford coefficients (r-values) computed for the ECAE material from TBH yield locus were used to determine the parameters of the Hill 1948 model:

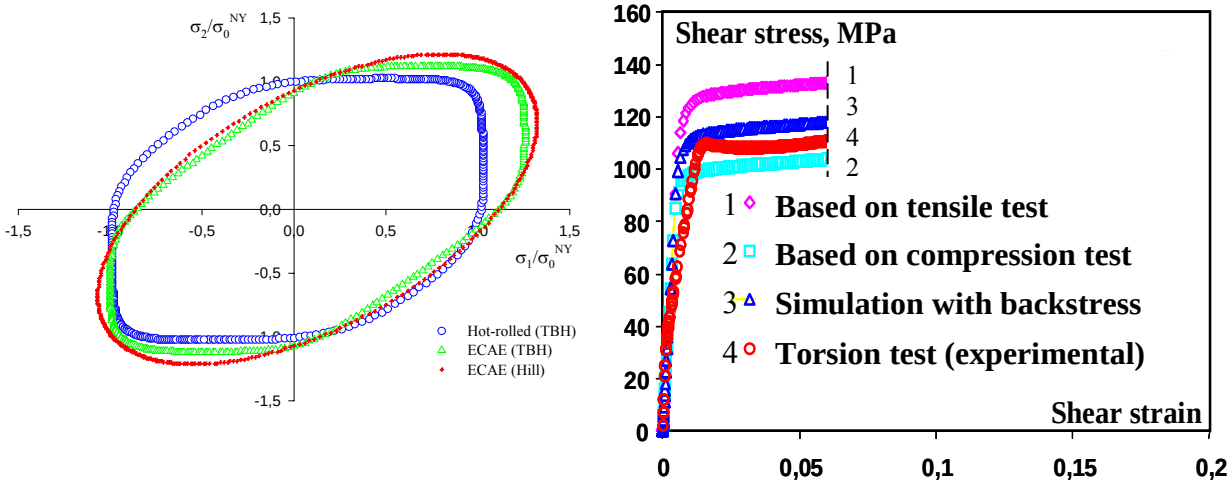

(a) (b)

Figure 2: (a) Initial yield locus for ECAE material and initial aluminum sheet; (b) Predicted shear stress-strain curves with Hill model scaled by different reference stresses, with and without back stress and experimental results.

$$f(\underline{\sigma}) = F(\sigma_{22} - \sigma_{33}) + G(\sigma_{33} - \sigma_{11}) + H(\sigma_{11} - \sigma_{22}) + 2L\sigma_{23} + 2M\sigma_{13} + 2N\sigma_{12} - 2\sigma_F . \quad (1)$$

where σ_{ij} are the Cauchy stress components, σ_F is the yield stress in a reference direction and state. The anisotropic shape of this yield surface is determined by the six material parameters *F*, *G*, *H*, *L*, *M* and *N*. In this study, F=0.94, G=0.65, H=1.35 and L=M=N=2.07. Figure 2a compares this Hill yield locus to the TBH one. One can verify that both models predict different behavior in the plane strain and bi-axial states.

To account for the large tension σ_y^t-compression σ_y^c asymmetry in strength caused by the ECAE process, a simple approach is chosen. The yield loci from Figure 2a are shifted by an initial back stress defined by experimental test results of Figure 1 ($(\sigma_y^t - \sigma_y^c)/2 = 21$MPa). The Hill yield locus shape and position is validated by the yield strength obtained in a torsion test. In Figure 2b, the cases 1 and 2 respectively show the stress strain curves computed by Hill model without back stress and with σ_F the initial flow stress in tension and compression. The case 3 is related to the Hill yield locus shifted by the back stress and with σ_F a mean reference stress ($(\sigma_y^t + \sigma_y^c)/2 = 164.2$ MPa). All these cases are coupled with an perfect elasto-plastic hardening model fitted on the compression curve shown in Figure 1a. The kinematic model used in case 3 is very limited as without further experimental work, the back stress evolution is unknown and is just kept constant.

3.2 Simulation of the compression test

Figure 3 defines the reference axes. The compression axis of the test specimen was aligned with the ECAE Extrusion Direction. Both the undeformed and 80% deformed test specimen shapes are presented in Figure 4. The deformed test specimens at 40% and 80% of uniaxial strain were optically measured and in Figure 4b the thick lines correspond to the actual cutting of the test specimen. The outer lines correspond to the (possible) test specimen edges. The middle line corresponds to the position of the horizontal midplane. FE simulations by Lagamine code are used to compare the final predicted and experimental test specimen shapes after compression tests. Two yield loci, coupled with the isotropic Voce model and with the constant back stress already identified above, have been applied to these simulations: Hill 1948 and the Minty micro-macro model which locally interpolates the stress-strain relation from yield locus points computed by a polycrystal Taylor model based on the initial texture description.

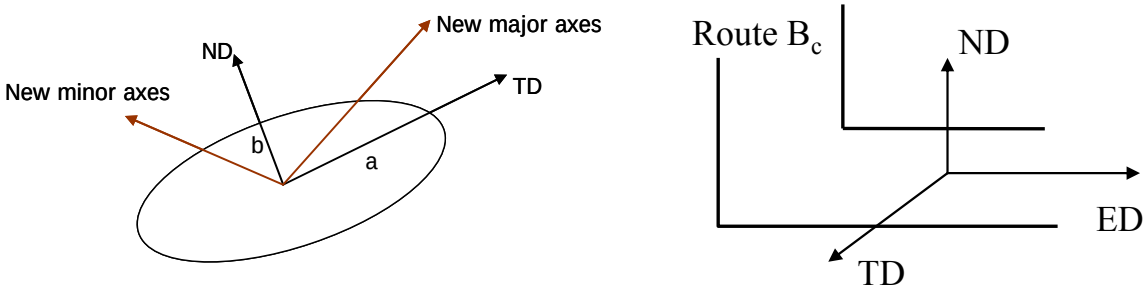

(a) (b)

Figure 3: Axes definition.

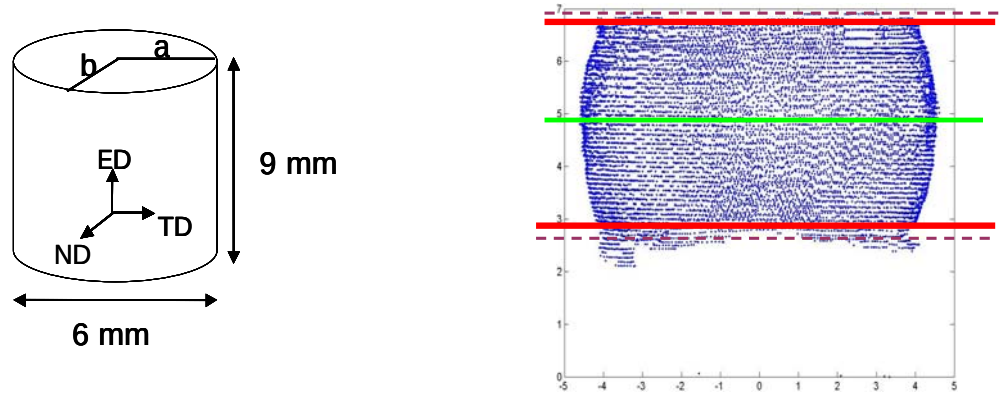

(a) (b)

Figure 4: (a) The original compression test specimen geometry; (b) profile measurement on 80% deformed compression test specimen.

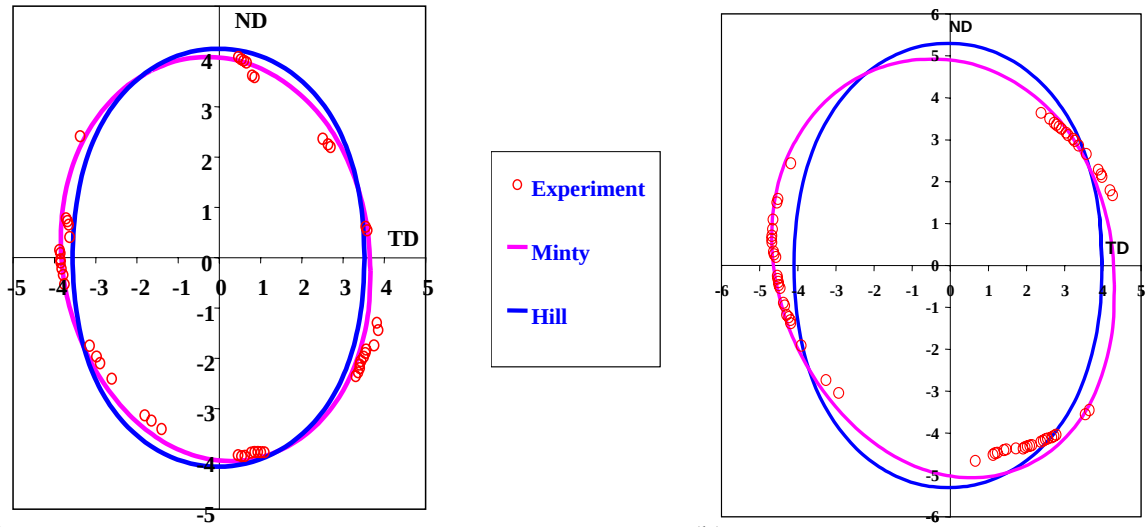

(a) (b)

Figure 5: Midplane measurement and simulation for compression on 40% (a) and 80% (b).

The Coulomb model was used to model the contact [6] and a friction coefficient of 0.1 allows predicting the measured barreling effect. Three dimensions mixed type elements [7] were used, half of the test specimen was meshed as no other symmetry than the horizontal midplane was assumed. Figure 5 compares the predicted and measured mid plane sections. As the Hill yield locus had been identified with the hypothesis that the Transversal and the Normal Directions were orthotropic axes, the Hill simulation predicts an elliptic shape in those directions (Figure 3a). The Minty yield locus was also identified in these axes but none symmetry was assumed. Its shape is clearly close from the actual yield locus of the ECAE material as it predicts both the elliptic shape and its rotation during the compression. Note that the Minty law does not take into account the texture evolution during the compression; it just uses the initial texture to define an accurate initial anisotropic yield locus.

3.3 Simulation of the tensile test

The geometry of the experimental tensile test specimens is drawn in Figure 6a, the diameter of the tested zone is 5mm when its length is 10mm. The current simulations use an axi-

symmetric state around Y-axis and a X-symmetry axis. Only the shaded part of the test specimen shown in Figure 6a is meshed with 484 BLZ2D elements [8]. Nodal displacements are prescribed at the upper part of the test specimen.

In a first attempt, the simulation goal was not the prediction of the exact shape of the deformed test specimen but the identification of a possible hardening behavior. The slowest tensile test (0.015mm/min) from Figure 1b was chosen as the curve shape suggests late necking and rupture. To describe the behavior of ECAE material during this tensile test, isotropic Von Mises law coupled with isotropic hardening is used. This first step already brings some knowledge before using an elasto-viscoplastic model closer to the actual behavior at these strain rates. Three types of hardening are checked: material law 1 presents material softening (directly computed from experimental force, homogeneous stress state and volume conservation), material law 2 is perfectly rigid-plastic and material law 3 has a hardening behavior (Figure 6b).

The load-displacement curves computed by the simulations are compared in Figure 7a for the three types of material laws studied. The results obtained show that the choice of the law has a strong effect on the necking appearance. The introduction of hardening in the law delays

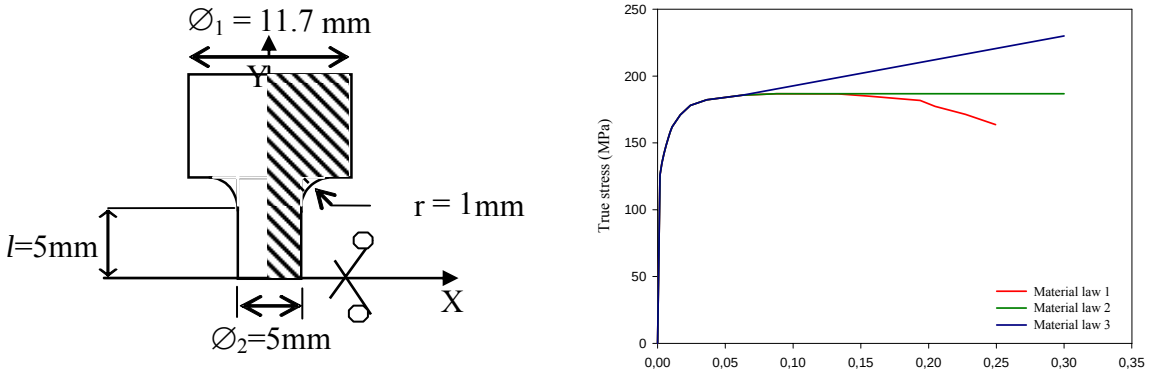

(a) (b)

Figure 6: (a) Size and shape of studied specimen; (b) Material laws introduced in Lagamine code for tensile tests.

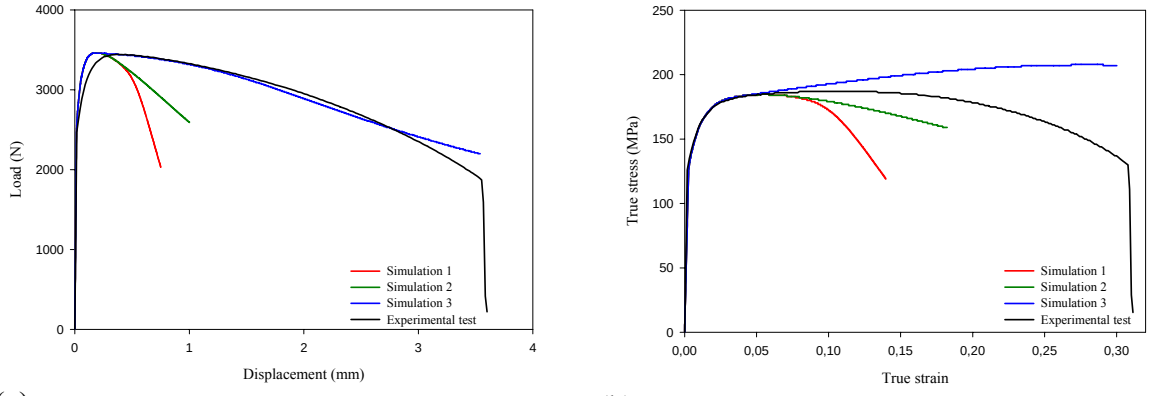

(a) (b)

Figure 7: (a) Load-displacement curves obtained by tensile test and simulation;
(b) True stress-true strain curves calculated from force and displacement data obtained by FE.

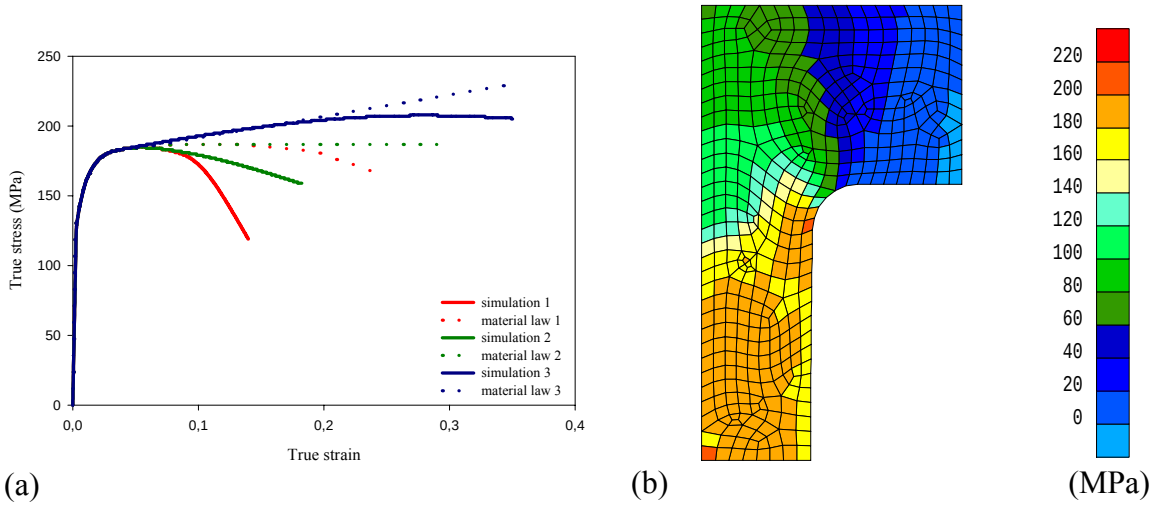

Figure 8: (a) True stress-strain strain curves either the input material laws or the computed ones from simulations force-displacement curve; (b) Stress field σ_Y (MPa) for a displacement of 0.16mm associated to a strain of 0.032.

necking. Thus, the curve from material law 3 approaches the behavior of the experimental curve. Figure 7b shows the associated true stress-true strain curves computed from the simulated and experimental load-displacement curves from Figure 7a assuming homogeneous deformation and volume preservation.

The curves from Figure 7b, deduced from the simulated reaction forces and assuming test homogeneity are compared with the input FE material laws used to compute these reactions in Figure 8a. The strong difference confirms that the stress is not at all homogeneous during the test. The stress field shows the test heterogeneity (Figure 8b). This result is not surprising as the test specimen geometry is far from the recommended tensile specimen shape where the length should be five times the diameter [9]. Clearly an inverse method coupling FE simulations with the experiments is required. One cannot propose a stress-strain curve for ECAE tensile behavior just by deriving stress from force measurement with the assumption of stress homogeneity.

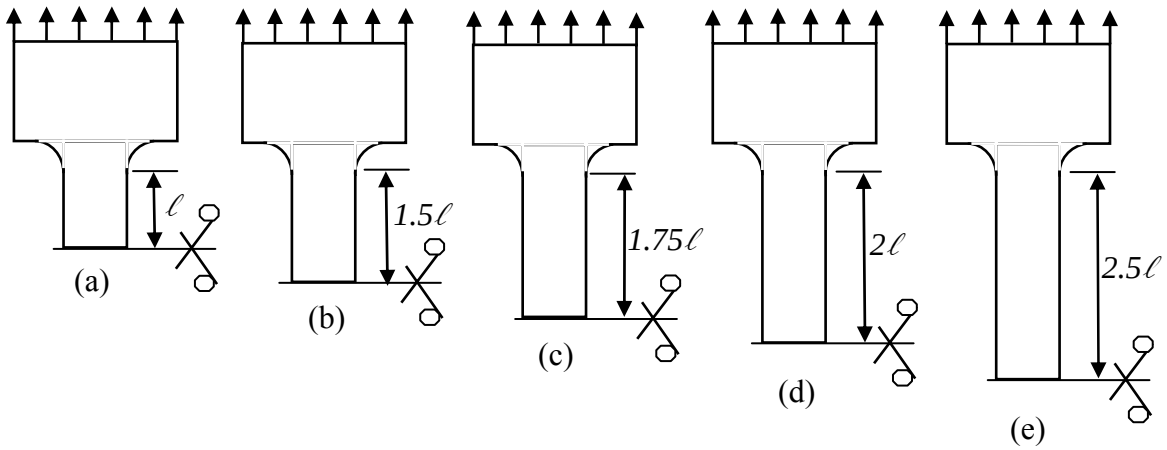

Figure 9: Different test specimen lengths: (a) Initial length ℓ ; (b) length $\ell \times 1.5$; (c) length $\ell \times 1.75$; (d) length $\ell \times 2$ and (e) length $\ell \times 2.5$

3.4 Length effect

Due to the way the ECAE test specimens are produced, it is quite impossible to follow the standards. So a numerical sensitivity analysis of the test specimen length has been performed with five test specimens of different lengths, referred as lengths 1, 1.5, 1.75, 2 and 2.5. The test specimen of length l corresponds to the test specimen shown in Figure 6a. The other test specimens are obtained by keeping the characteristic dimensions and multiplying the length of the specimen by a length factor (Figure 9). Moreover, the analysis was carried out in the case of the material laws 1 (with softening) and 3 (with hardening), the FE size has been kept so that the simulation mesh of length $2.5l$ has a larger number of elements.

The load-displacement and true stress-true strain curves derived from the simulations (assuming stress homogeneity) are plotted in Figures 10 and 11 respectively for the material laws 1 and 3. These figures show that the increase of the length of test specimens leads to different slopes of necking. Values reported in Tables 1 and 2 show that level of maximum Force is almost identical. The Considere criterion [10] tells that "possible necking" appears at the curve maximum (necessary condition but not sufficient). It is interesting to note that FE simulations predict this maximum in a weak interval of strains ($0.03245 \leq \varepsilon \leq 0.03343$) for all the test specimen lengths higher than length l (case of test specimens (b), (c), (d) and (e) in Figure 9) for material laws 1 and 3. The length l provides a strain outside this range, probably because this test specimen shape provides larger stress gradient in the test specimen than all the other test specimens. It has to be noted that, in Figure 9, case (e) is the first geometry which is close to the standards. Current ECAE process does not provide long test specimen which prevents to follow the normative rules requiring a length larger than five diameters of the test specimen.

Looking at Figures 10b and 11b, the test specimens with the smaller length seem to delay the localization. As the test homogeneity is not fully respected for small lengths, this conclusion could not be reliable. However careful analysis of Figures 10a and 11a related to force confirms that the necking slope (angle α) is higher for longer tests specimens.

To analyze these results from a theoretical point of view, a uniaxially loaded test specimen is considered as shown in Figure 12. Here an extreme behavior law with localization is assumed (Figure 13a).

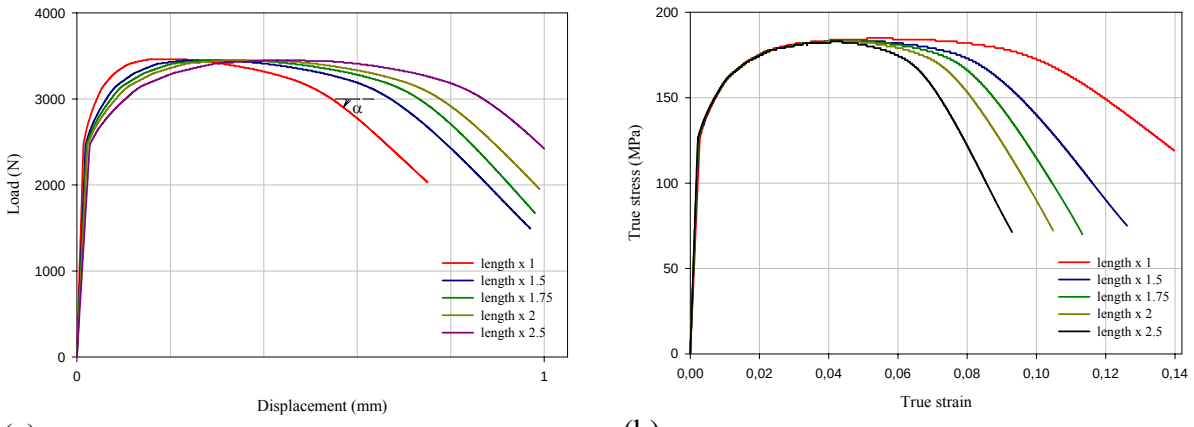

(a) (b)

Figure 10: (a) Load-displacement curves obtained by simulation with five different lengths of test specimen using material law1 (law with softening); (b) True stress-true strain curves computed from simulated forces and displacements given by Figure 10a.

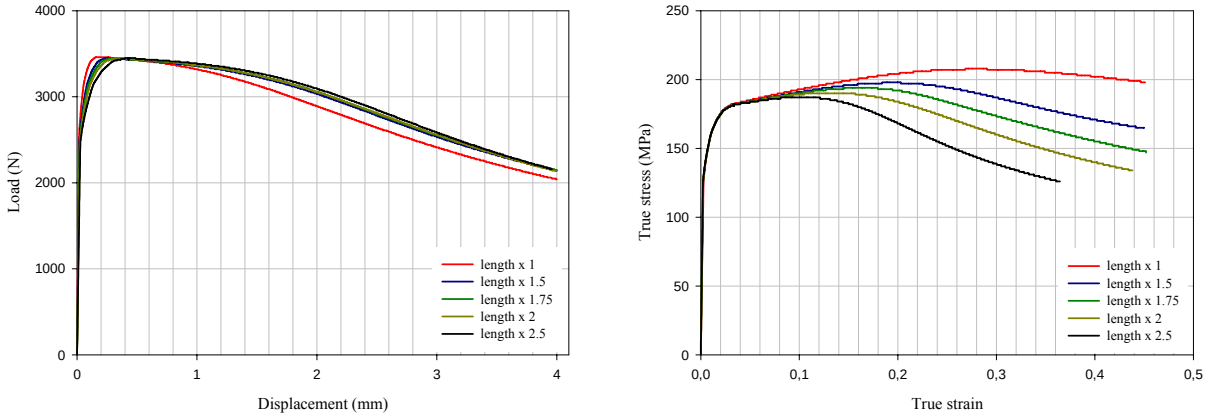

Figure 11: (a) Load-displacement obtained by simulation with five different lengths of test specimen using material law3 (law without softening but hardening); (b) true stress-true strain computed from force and displacement given by Figure 11a.

Length	Max load (N)	Max displacement (mm)	Associated max strain
l	3461.47	0.1856	0.03640
1.5 *l*	3450.92	0.2474	0.03245
1.75 *l*	3452.59	0.2885	0.03244
2 *l*	3452.42	0.3337	0.03282
2.5 *l*	3452.37	0.4250	0.03343

Table 1: Values of the "possible beginning" of necking for five different lengths of test specimen from material law 1 (with softening)

Length	Max load (N)	Max displacement (mm)	Associated max strain
l	3461.47	0.1856	0.03640
1.5 *l*	3450.92	0.2474	0.03245
1.75 *l*	3452.59	0.2885	0.03244
2 *l*	3452.42	0.3337	0.03282
2.5 *l*	3452.06	0.4255	0.03379

Table 2: Values of the "possible beginning" of necking for five different lengths of test specimen from material law 2 (no softening, with hardening).

Let us remind some theoretical bases: in small deformations, for elasto-plastic stress-strain curve with softening, analysis of bifurcation predicts necking. For stress-strain curve with hardening, no necking is predicted. While in large deformations due to volume conservation, the test specimen section decreases and the load-displacement curve presents a softening even with stress-strain curve without softening. According the relative rate of hardening compared to the effect of section decrease, necking can happen. Of course, it always happens later than with softening materials.

The length (L+*l*) of the bar has been chosen. One assumes that a strain concentration appears in the part noted 2 in Figure 12.

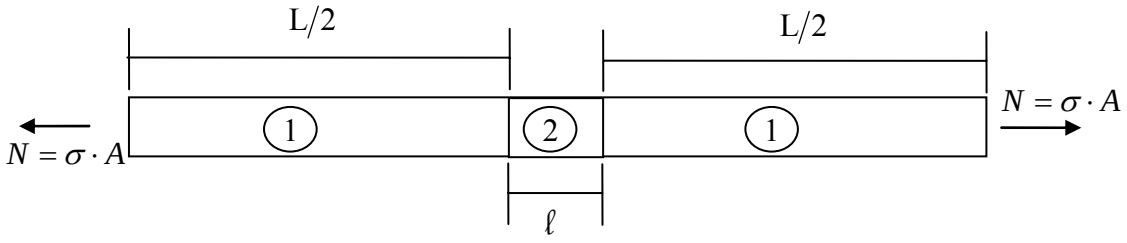

Figure 12: Uniaxially loaded test specimen.

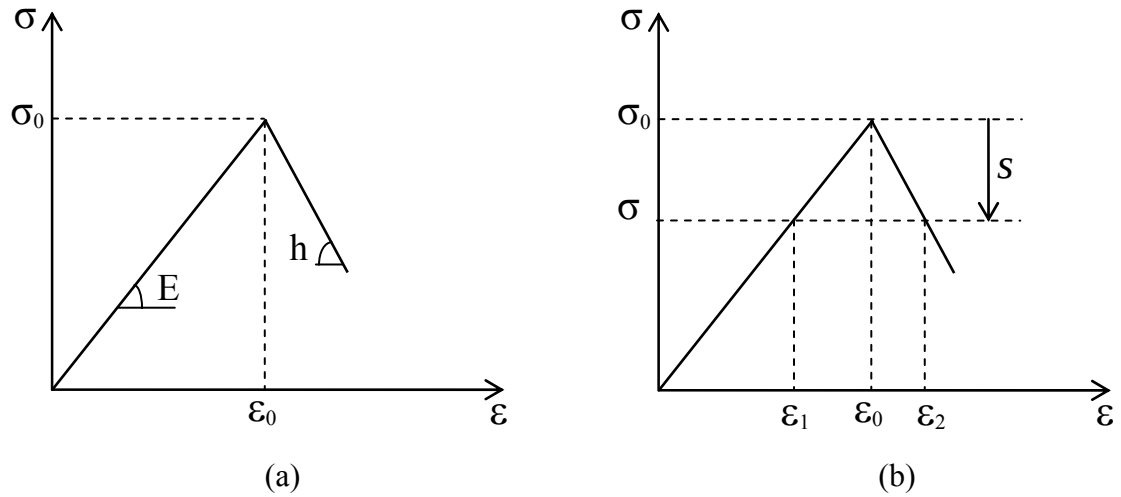

Figure 13: Behavior law with localization

Before localization i.e $\varepsilon < \varepsilon_0$, everywhere in the test specimen, the stress is given by:

$$\sigma = \mathrm{E}\varepsilon \,. \tag{2}$$

Let us note Δ the displacement when necking occurs with a different strain in part 1 and 2 of the test specimen,

$$\Delta = \varepsilon\left(L + l\right), \tag{3}$$

then using relation (2), the expression of Δ becomes,

$$\Delta = \frac{\sigma}{E}\left(L + l\right). \tag{4}$$

After localization (see Figure 13b), the force equilibrium provides in parts noted 1:

$$\Delta_1 = L\varepsilon_1 = L\frac{\sigma}{E} = L\left(\frac{\sigma_0}{E} - \frac{s}{E}\right), \tag{5}$$

and in the middle part of the bar noted 2:

$$\Delta_2 = l\varepsilon_2 = l\left(\varepsilon_0 - \frac{s}{h}\right) = l\left(\frac{\sigma_0}{E} - \frac{s}{h}\right). \tag{6}$$

Thus the total displacement is

$$\Delta = \Delta_1 + \Delta_2 = (L + l)\frac{\sigma_0}{E} - s\frac{L}{E} + s\frac{l}{h} \tag{7}$$

where s is identified in Figure 13b. If Δ_{loc} is the displacement when localization happens,

$$\Delta_{loc} = \Delta(s = 0) = (L + l)\frac{\sigma_0}{E}, \tag{8}$$

the displacement after necking can be expressed by:

$$\Delta = \Delta_{loc} + s\frac{l}{h} - s\frac{L}{E} \tag{9}$$

From equation(9), at a given s (see Figure 14 a), it can be written:

$$\Delta - \Delta_{loc} = s\left(\frac{l}{h} - \frac{L}{E}\right). \tag{10}$$

If the curve slopes before and after localization are equal i.e $h = E$, the preceding relation (10) becomes,

$$\Delta - \Delta_{loc} = \frac{s}{E}(l - L) = \frac{sL}{E}(\xi - 1), \tag{11}$$

where $\xi = \frac{l}{L}$ is the ratio between the length of the part called 2 and the length of the remainder of the bar. Now a direct analysis of the test specimen length is possible: if the length of part 2 is less than the length of part 1 ($l < L$), the quantity $\Delta - \Delta_{loc}$ is negative. For example, considering some particular cases given in Figure 14b,

- Case (a) : when $l = 0{,}1\,L$ then $\xi = 0{,}1$ and $\Delta - \Delta_{loc} = -\frac{0{,}9\,sL}{E}$
- Case (b) : when $l = L$ then $\xi = 1$ and $\Delta - \Delta_{loc} = 0$
- Case (c) : when $l = 2\,L$ then $\xi = 2$ and $\Delta - \Delta_{loc} = \frac{sL}{E}$

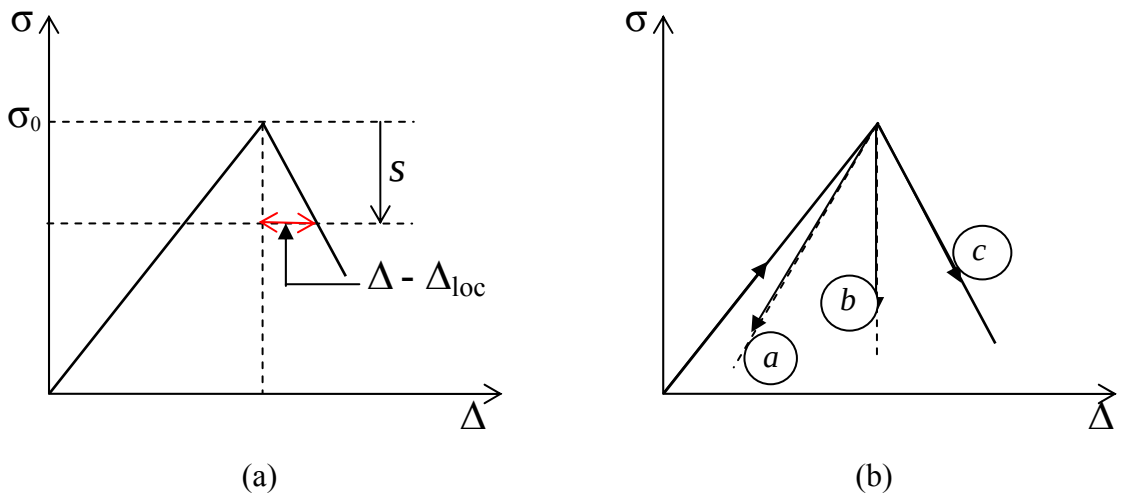

(a) (b)

Figure 14- Behavior laws with localization.

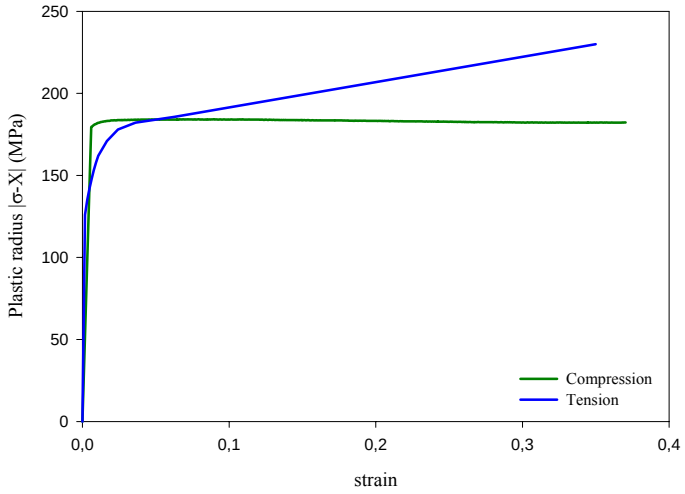

Figure 15: Plastic radius in tension and compression.

This simplified demonstration neglecting large strains predicts that for a negative slope (material law 1). When the test specimen length increases, the ratio ξ between the necking zone length (typically one finite element for non diffuse necking as observed in the simulations) and the length of the test specimen decreases and the slope ($\sigma - \Delta$) of the necking is reduced (see Figure 14b: from case c to case b and case b to case a).

So this demonstration confirms that Figure 10b results are consistent with the theory. In the finite element model considered in this study, the problem is not totally similar to this simplified approach. The material law 1 has a plateau before softening behavior and not a maximum reduced to one point, the simulations are in the large deformations range. However quite similar results are recovered: the maximum strain predicted by simulation stays in a small range of strains and the predicted necking slope is higher for larger test specimen length.

3.5 Isotropic strain hardening

Even if a better identification can be performed by inverse modeling with tensile experiments, it can be interesting to compare the tensile material law predicting correctly the force curve (material 3 on Figure 7a) with the stress-strain curve used to model the compression test. Assuming a constant back stress of 21 MPa, Figure 15 shows the plastic radius in tension and compression. Clearly the hardening rate is different for both loading states. This behavior has to be inserted either in the evolution rule of back stress or in the isotropic hardening model.

4 CONCLUSIONS AND PERSPECTIVES

First phenomenological models to evaluate the behavior of ultrafine-grained aluminum produced by ECAE process submitted to tension, compression and torsion exist. They must be developed and validated by other experiments. The results obtained show that an anisotropic Hill function with a proper initial back stress is able to recover the initial flow stress in tension, compression and torsion. In compression test, the predicted shape of the cross section of a compressed test specimen by Minty model, coupled with a Voce-type hardening model, gives the best agreement with the experimental results. Tensile tests simulations clearly confirm that the stress state cannot be automatically derived from the measured force because of

the inhomogeneity of stress field during the test. This problem is due to the geometry of the test specimen produced by ECAE process which is far of standards recommendation.

The present study is restricted to the analysis of tensile test with an elasto-plastic law. However, the results obtained clearly show the capacity of this model to analyze the stress state through the test specimen. Furthermore, it would be necessary to extend the study to an inverse modeling for tensile experiment with an elasto-plastic model for tests performed at higher strain rates and with an elastovisco-plastic model for tests performed at slower strain rates. It would be also interesting to experimentally look at the evolution of kinematic work hardening by performing tensile test followed by compression one. The final goal is to develop one model able to simulate the two types of monotonous tests, tension and compression, and to validate it by torsion test simulations but also complex tests such as tension-torsion tests.

ACKNOWLEDGEMENT

This study was carried out in the frame of project IAP, P5/08 financed by Belgian Science Policy. A.M. Habraken is mandated by the National Fund for Scientific Research (Belgium).

REFERENCES

[1] S. Poortmans, B. Verlinden, Thermal stability of CP-aluminum during annealing after ECAE. *Materials Science Forum*, **467-470**, 1319–1324, 2004.

[2] G. E. Dieter, *Mechanical Metallurgy.* 3 rd Ed., McGraw-Hill Book Co., London, 1986.

[3] A.M. Habraken, S. Cescotto, An Automatic Remeshing Technique for Finite Element Simulation of Forging Processes. *International Journal of Numerical Methods in Engineering*, **30**, 1503–1525, 1990.

[4] A. M. Habraken, L. Duchêne, Anisotropic elasto-plastic finite element analysis using a stress-strain interpolation method based on a polycrystalline model. *International Journal of Plasticity*, **20**, Issue 8-9, 1525–1560, 2004.

[5] P. Van Houtte, A comprehensive mathematical formulation of an extended Taylor-Bishop-Hill model featuring relaxed constraints, the Renouard-Wintenberger theory and a strain rate sensitivity model. *Texture and Microstructure*, **8-9**, 313-350, 1988.

[6] S. Cescotto, A.M. Habraken, Contact between Deformable Solids the Fully Coupled Approach, *Journal of Mathematical and Computer Modelling*, **Special Issue**, 1988.

[7] Y.Y. Zhu, S. Cescotto, Unified and mixed formulation of the 8-node hexahedral elements by assumed strain method. *Computer Methods in Applied Mechanics and Engineering,* **129**, 177–209, 1995.

[8] Y.Y. Zhu, S. Cescotto, Unified and mixed formulation of the 4-node quadrilateral elements by assumed strain method. *International Journal of Numerical Methods in Engineering,* **38**, 685–716, 1990.

[9] European norm. EN 10002-1, Metallic materials - Tensile testing- Part 1: Method of test. Institut belge de normalisation, Brussels, 1992.

[10] J.W. Hutchinson, K.W. Neale, Influence of strain-rate sensitivity on necking under uniaxial tension. *Acta Metallurgica*, **25**, 839–846, 1977.